LANGMUIR

pubs.acs.org/Langmuir Article

Electrosteric Control of the Aggregation and Yielding Behavior of Concentrated Portlandite Suspensions

Sharu Bhagavathi Kandy,* Narayanan Neithalath, Mathieu Bauchy, Aditya Kumar, Edward Garboczi, Torben Gaedt, Samanvaya Srivastava, and Gaurav Sant*

Cite This: *Langmuir* 2023, 39, 10395−10405 Read Online

ACCESS | Metrics & More | Article Recommendations | Supporting Information

ABSTRACT: Portlandite (calcium hydroxide: CH: $Ca(OH)_2$) suspensions aggregate spontaneously and form percolated fractal aggregate networks when dispersed in water. Consequently, the viscosity and yield stress of portlandite suspensions diverge at low particle loadings, adversely affecting their processability. Even though polycarboxylate ether (PCE)-based comb polyelectrolytes are routinely used to alter the particle dispersion state, water demand, and rheology of similar suspensions (e.g., ordinary portland cement suspensions) that feature a high pH and high ionic strength, their use to control portlandite suspension rheology has not been elucidated. This study combines adsorption isotherms and rheological measurements to elucidate the role of PCE composition (i.e., charge density, side chain length, and grafting density) in controlling the extent of PCE adsorption, particle flocculation, suspension yield stress, and thermal response of portlandite suspensions. We show that longer side-chain PCEs are more effective in affecting suspension viscosity and yield stress, in spite of their lower adsorption saturation limit and fractional adsorption. The superior steric hindrance induced by the longer side chain PCEs results in better efficacy in mitigating particle aggregation even at low dosages. However, when dosed at optimal dosages (i.e., a dosage that induces a dynamically equilibrated dispersion state of particle aggregates), different PCE-dosed portlandite suspensions exhibit identical fractal structuring and rheological behavior regardless of the side chain length. Furthermore, it is shown that the unusual evolution of the rheological response of portlandite suspensions with temperature can be tailored by adjusting the PCE dosage. The ability of PCEs to modulate the rheology of aggregating charged particle suspensions can be generally extended to any colloidal suspension with a strong screening of repulsive electrostatic interactions.

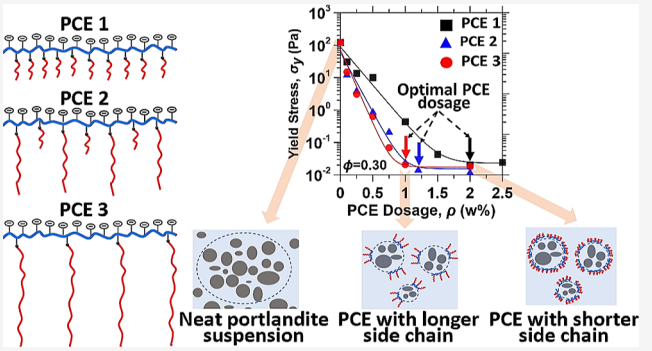

INTRODUCTION AND BACKGROUND

Calcium hydroxide [CH: $(Ca(OH)_2$], also known as portlandite, slaked lime, or hydrated lime, is an industrially relevant mineral that finds extensive applications in the food processing industry,[1] water treatment,[2,3] construction,[4] carbon dioxide mineralization,[5−7] and dentistry.[8] Due to their modest solubility and quick dissolution rate, portlandite suspensions have a self-regulating pH (∼ 12.6) that is close to their isoelectric point (IEP ∼ 13) and a comparatively high ionic strength (I ∼ 60 mmol/L), causing effective screening of any repulsive electrostatic interactions between portlandite particles. Consequently, portlandite particles aggregate spontaneously and form fractal networks when dispersed in water.[9,10] As a result, the yield stress (σ_y) and apparent viscosity (η) of portlandite suspensions diverge at relatively low solid volume fractions (ϕ), adversely affecting flowability, causing jamming, and severely limiting the maximum achievable solid volume fraction prior to the onset of jamming (i.e., $\phi_m \sim 0.35$).[11,12] Additionally, increasing temperature further weakens the electrostatic repulsion between the portlandite particles, triggering quicker aggregation and the creation of larger aggregates.[10] This temperature-induced aggregation produces an unusual rheological response, complicating processability when subjected to changing (non-isothermal) conditions.

To ensure the flowability and processability of portlandite suspensions while simultaneously maximizing particle loading ϕ_m, it is essential to minimize particle aggregation and reduce σ_y using appropriate dispersants. Generally, suspension rheology is controlled by introducing repulsive interactions between particles by various methods, such as increasing the surface charge (i.e., electrostatic interactions),[13] adsorbing or attaching polymers to the particle surfaces to create steric hindrance,[9,14] or a combination of both.[15−18] However, due to

Received: March 14, 2023
Revised: July 1, 2023
Published: July 18, 2023

https://doi.org/10.1021/acs.langmuir.3c00704
Langmuir 2023, 39, 10395−10405

the particular characteristics of portlandite suspensions (i.e., high pH and ionic strength), comb polyelectrolytes are more effective in tuning their rheology when compared to linear polyelectrolyte dispersants at similar ϕ.[9] Polycarboxylate ether (PCE)-based comb polyelectrolyte dispersants have been widely used to mitigate particle aggregation in similar systems featuring high pH and high ionic strength, particularly in cementitious suspension, such as concrete.[19,20] PCE comb polyelectrolytes often comprise a main chain (i.e., backbone) holding carboxylate anions and multiple non-ionic side chains of polyethylene glycols or a combination of polyethylene/polypropylene oxides.[21] The excellent dispersing effect of PCEs is attributed to the steric screening of the attractive interparticle van der Waals interactions by the comb polyelectrolytes that adsorb onto the particle surfaces.[22,23] The higher adsorbed layer thickness and steric hindrance introduced by comb polyelectrolytes effectively limit portlandite particles' fractal structuring and regulate suspension rheology.[9]

While commercially available PCEs effectively alter the particle dispersion state and rheology of portlandite suspensions,[9,24] the crucial attributes of how PCEs influence portlandite suspension rheology remain unexplored. Herein, we explore the correlations between the side chain length of PCEs and the macroscopic rheological characteristics of portlandite suspensions. We combine adsorption isotherms and rheological measurements to elucidate the role of the non-ionic side chain length of PCEs in controlling the extent of adsorption, flocculation state, and yielding characteristics of portlandite suspensions. We also elucidate the role of the chemical structure and dosage of PCEs in moderating the temperature-dependent rheology of portlandite suspensions. By delineating the role of the PCE dispersant's chemical structure in controlling the rheology of colloidal suspensions that feature high ionic strength and strong charge screening behavior, the outcomes of this study provide general insights regarding dispersant selection for such (high pH and high ionic strength) applications.

MATERIALS AND METHODS

Materials. The commercial portlandite powder, Standard Hydrated Lime (density = 2340 kg/m^3), was obtained from Mississippi Lime[a]. The purity of portlandite was established to be 94.8 ± 0.5% based on thermogravimetric analysis (TGA), with calcium carbonate ($CaCO_3$) accounting for the remainder. The particle size distribution of the portlandite particulates was obtained using static light scattering (Partica LA-960A2, Laser Scattering Particle Size Distribution Analyzer, Horiba) on dilute suspensions (0.002 vol %) of the particles in a saturated calcium hydroxide solution. The median particle size d_{50} (i.e., the radius of gyration) of the commercial portlandite powder was calculated to be 4.6 ± 0.1 μm (Figure S1a in the Supporting Information). Scanning electron microscopy analyses (FEI Nova NanoSEM 230 FE-SEM) of the portlandite particulates revealed they were composed of aggregates of tiny primary $Ca(OH)_2$ particles, as depicted in Figure S1b. Further, transmission electron microscopy (FEI T12 Quick CryoEM) analyses estimated the diameter of the primary portlandite particles to be between 20 and 200 nm (details can be found elsewhere[10]). The SEM images showed a size distribution comparable to that determined by static light scattering. The specific surface area of the portlandite particles was measured using Brunauer−Emmett−Teller analysis to be 12.54 ± 1.2 m^2/g. Three experimental-grade PCE dispersants were provided by Master Builders Construction Chemicals, named PCE 1, PCE 2, and PCE 3, in increasing order of their side chain lengths. One commercial-grade superplasticizer was also studied for comparison and named PCE MG (i.e., Master Glenium 7500, Master Builders Construction Chemicals). It should be noted that the experimental-grade PCEs are pure PCEs dispersed in water, while PCE MG is a commercial formulation containing functional additives, wherein the exact formulation is proprietary. The zeta potential of portlandite particles was found to be +18 ± 2 mV when they were dispersed in saturated calcium hydroxide solution, and the charge was reversed when PCEs were present. At the saturation dosage of PCE, the zeta potential ζ lies between 0 and −10 mV for the different PCE structures.

Characterization of PCEs. The dispersants' pH, specific gravity, solid content, molecular weight, and charge density were measured. Additionally, the dispersants were characterized using Fourier transform infrared and Proton nuclear magnetic resonance (^{1}H NMR) spectroscopy analyses. A generic chemical structure of the studied PCE dispersants, based on the Gay and Raphaël model,[25] and the schematic representations of each PCE dispersant are shown in Figure 1. According to the model, PCEs comprise n repeating

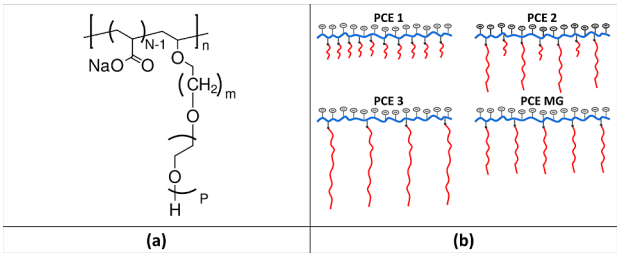

Figure 1. (a) Generic molecular structure of PCE dispersants used in the present study. It contains n repeating units with N monomers in the backbone, and each segment includes one side chain with P monomers. (Note: the exact nature of vinyl-ether-PEO is unknown, and m is the no. of methylene groups in the vinyl-ether-PEO side chains and is often in the range of 1−4; here, m is assumed to be 2, and this assumption does not significantly impact the estimated structural parameters). (b) Schematic representations of the four PCE dispersants (adapted from[26]).

structural units, each containing a backbone with N monomers and a side chain attached to it with P monomers (Figure 1a). The backbone of the anionic comb polyelectrolytes is composed of the sodium salt of polyacrylic acid (PAA-Na) and neutral vinyl polyethylene oxide side chains. The size of the side chains was 1100 g/mol, a mixture of 1100 and 3000 g/mol variants, 5800, and 3000 g/mol for PCE 1, PCE 2, PCE 3, and PCE MG, respectively.

Table 1 lists the composition and molecular weights along with the structural parameters corresponding to the Gay and Raphaël model (i.e., n, N, and P) of the dispersants used in this study. These parameters have been estimated using the generic chemical structure of PCEs (Figure 1a), the measured molecular weights, and charge density. Since PCE 2 comprises side chains with two different lengths (i.e., 1100 and 3000 g/mol) and their relative fraction is unknown, we assumed a 50−50 mass fraction to estimate its structural parameters. The solid content of the PCE 1, PCE 2, PCE 3, and PCE MG solutions was determined as 44.0, 51.2, 44.4, and 26.6 mass %, respectively. All four dispersants possessed identical charge densities at pH 12 ($C_d \sim$ 33−45 eq/mol) but different side chain lengths and grafting densities. The carboxylate-to-ether ratio (i.e., C/E ratio) of the PCEs are 2.4, 5.4, 6.8, and 3.7 for PCE 1, PCE 2, PCE 3, and PCE MG, respectively. The dispersity ($Đ$) for all four PCEs is between 1.5 and 2.

PCE Adsorption. The total organic carbon (TOC) analyzer (TOC-L, Shimadzu) was used to assess the absorption characteristics of the different PCE dispersants on portlandite surfaces. Adsorption measurements were performed using dilute suspensions (5 vol %) with varied PCE dosages (up to 5% of the dry mass of PCE by mass of portlandite). A non-purgeable organic carbon (NPOC) analysis was done to prevent an overestimation of the inorganic carbon because of

https://doi.org/10.1021/acs.langmuir.3c00704
Langmuir 2023, 39, 10395−10405

Table 1. Characteristics of the PCE Dispersants Studied Herein, Including Estimated Values of Their Structural Parameters

	side chain MW (g/mol)	M_n (g/mol)	M_w (g/mol)	$Đ\left(\frac{M_w}{M_n}\right)$	C_d (μeq/mol)	N	P	n
PCE 1	1100	23,400	40,500	1.73	42	3.4	25	17.4
PCE 2	2050*	18,400	26,600	1.45	39	6.4	46	7.4
PCE 3	5800	30,800	53,500	1.73	33	7.8	131	4.9
PCE MG	3000	40,500	74,800	1.85	45	4.7	68	12.1

*PCE 2 comprises side chains with two different lengths (i.e., 1100 g/mol and 3000 g/mol), and their relative mass fraction is proprietary. Hence, we assumed a 50−50 mass fraction of both lengths and an average side chain length of 2050 g/mol.

the formation of calcium carbonate ($CaCO_3$). The adsorbed amount of PCEs was determined by the solution depletion method. The amount of PCE remaining in the solution was first estimated by separating the liquid phase from the suspension. The adsorbed amount was calculated using a mass balance based on the amount of polymer initially added. Each dispersant was calibrated by testing a series of known concentrations of dispersants to correlate the NPOC concentration to the dispersant concentration. More details on the sample preparation for adsorption measurements can be found elsewhere.[9] We note that a fraction of PCE chains may remain trapped between the particles after the centrifugation, and hence, to be precise, TOC measurements estimate the amount of PCEs "consumed" instead of "adsorbed." Three aliquots of each sample were tested, and an average value was reported.

Preparation of Suspensions for Rheology Assessments. 50 mL of portlandite suspensions were prepared in saturated portlandite solutions with solid volume fractions (ϕ) varying from 0.10 to 0.50. The dispersant dosage ρ was varied between 0.1 and 2.5% dry mass of PCE to the mass of portlandite particles. To prepare suspensions, PCE dispersants (when applicable) were added to the saturated portlandite solution, followed by adding portlandite particles. The mixture was stirred thoroughly for 300 s at 500 rpm employing a four-bladed impeller-type blender (RW 20 Digital, IKA) to obtain a homogenous suspension.

Rheology. Rheology measurements were conducted with freshly prepared suspensions using a TA Instruments Discovery HR-2 rheometer with a four-bladed vane in cup geometry. The rheometer was set up with a Peltier concentric cylinder jacket for temperature regulation and had a solvent trap to reduce water vaporization. The rheology of portlandite suspensions was investigated through shear rotary and dynamic oscillatory measurements with different testing protocols to assess their flow curves, viscoelastic character, and temperature-dependent behavior. Following suspension loading and temperature equilibration, it was pre-sheared for 60 s at a strain rate of 100 s^{-1} in order to make the suspension homogenous and get rid of any shear history effects. Subsequently, the shear rate was decreased to 0.001 s^{-1} and maintained for 30 s to allow for the relaxation. Both ascending and descending shear rates ($\dot{\gamma}$) sweeps in logarithmic intervals, with 6 points per decade, from $\dot{\gamma}$ = 0.001 to 200 s^{-1} were performed with a 10 s averaging period for obtaining the flow curves. The rheological parameters (i.e., yield stress, σ_y and shear-thinning index,x) were then determined from the ascending shear rate sweep measurements. For suspensions that exhibit clear yielding characteristics, the stress corresponding to the flow curve's first yielding event was considered the yield stress. The flow curves were fitted with the Herschel−Bulkley model to obtain the yield stress for suspensions that exhibited subdued yielding (i.e., suspensions without a clearly definable yield stress). The Herschel−Bulkley model fits the rheological data better than the commonly used Bingham model. A few suspensions with a higher PCE dosage showed nearly Newtonian behavior (i.e., no signs of even subdued yielding), and their yield stress was assumed to be zero. A measure of the degree of shear-thinning was extracted by applying a power-law model, $\eta = k\dot{\gamma}^x$ where η is the apparent viscosity, k is the flow consistency index, and x is the shear-thinning index, to the data points that presented a linear trend in the $\eta-\dot{\gamma}$ curves (i.e., usually at intermediate $\dot{\gamma}$ values from a few s^{-1} to tens of s^{-1}). The estimation of σ_y and x from the flow curves is illustrated in Figure S2a,b provided in the Supporting Information. Sigmoidal fits were applied to the x and σ_y evolutions to estimate the optimal PCE dosage that is required for rheology modification (see Figure S2c in the Supporting Information for the details depicting the estimation of optimal yield stress from the evolution of x with increasing PCE dosage).

Oscillatory strain amplitude (γ) sweep measurements from γ = 0.001% to γ = 1000% at a frequency of 0.5 Hz were conducted to study the viscoelastic characteristics of the suspension. To elucidate the temperature-induced variations in the rheological responses of the suspensions, the shear rate sweep and dynamic amplitude sweep measurements were carried out at 25, 50, and 75 °C, with a precision of ±0.1 °C for each temperature. Prior to conducting rheological tests at different temperatures, we allowed a waiting period of ∼30 min for the suspension placed in the cup to reach the set temperature, which was monitored with a thermocouple probe. The TGA (STA 6000, PerkinElmer) was used to measure the extent of water evaporation and carbonation of portlandite in suspensions during the rheology measurements. The results confirmed that the rheological characteristics were not impacted by the evaporation of water and/or the carbonation of portlandite during the tests. In general, at least two unique samples were prepared and tested for each suspension. The rheology data reported is not impacted by particle settling, as precautions were taken to reduce the effects of particle sedimentation on the results.

RESULTS AND DISCUSSION

Adsorption Characteristics of PCE Dispersants. The adsorption behavior of dispersants on the particle surface is one of the fundamental parameters that affect suspension rheology.[27,28] The adsorption of a PCE onto solid surfaces is affected by its structural characteristics:[26] backbone chemistry and length, side chain grafting density (i.e., C/E ratio), and the size of the side chains.[17,26,29−31] The PCE's adsorption and adsorbed conformations largely control the effectiveness of PCEs as a plasticizer.[32] Previous studies on the conformational behavior of the PCEs in solution[33,34] and on different particle surfaces, including cement,[33] magnesium oxide,[35] and calcium-silicate-hydrate,[33] indicate that the solution pH, ionic strength, and the valence of the counter ions all influence the PCE's coil dimensions.[32,36] However, for PCEs grafted with PEO derivatives, the impact of pH and ionic strength of the medium on their conformation seems to be drastically lower than for polyelectrolytes like polyacrylic acid.[32] The side chains of PCEs often tend to be coiled when adsorbed onto a surface, and the adsorbed layer thickness is of the order of a few nanometers.[37]

Following the Gay and Raphaël model,[25] all four dispersants studied here belong to the flexible backbone worm conformation regime in solutions (i.e., a chain of cores, each having a radius of gyration R_g). Building on the work by Gay and Raphaël based on the minimization of the Flory free energy,[25] Flatt et al.[33] derived analytical expressions in terms of structural parameters P, N, and n for the conformation of PCEs in solutions (i.e., the radius of gyration R_g, eq 1) and adsorbed

https://doi.org/10.1021/acs.langmuir.3c00704
Langmuir 2023, 39, 10395−10405

on a cement particle (i.e., the adsorbed layer thickness and the surface occupied). PCEs are assumed to behave as a chain of hemispheres with the radius of hemispheres, R_{AC}, which indicates the adsorbed layer thickness shown in eq 2. Also, the surface occupied by each PCE molecule on a particle, S_A, can be calculated using eq 3.

$$R_g = \left(\left(\frac{a_N}{a_P}\right)^2 \frac{(1 - 2\chi)}{2}\right)^{1/5} a_P P^{2/5} N^{1/5} n^{3/5} \quad (1)$$

$$R_{AC} = \left(2\sqrt{2}(1 - 2\chi)\frac{a_P}{a_N}\right)^{1/5} a_P P^{7/10} N^{-1/10} \quad (2)$$

$$S_A = \frac{\pi}{\sqrt{2}} a_N a_P \left(2\sqrt{2}(1 - 2\chi)\frac{a_P}{a_N}\right)^{2/5} P^{9/10} N^{3/10} n \quad (3)$$

where a_N is the size of the monomers in the backbone, a_P is the size of the monomers in the side chains, and χ is the Flory parameter of the side chains. For specific assumptions, the scaling law was extended to estimate the adsorption equilibrium constant K_A (i.e., the ratio between adsorption and desorption rates at equilibrium) as a function of the PCE molecular structure[38]

$$K_A = \frac{z^2(N - 1)^2}{nP^{9/5}N^{3/5}} \quad (4)$$

where z is the number of charges each monomer carries in the backbone. With this adsorption equilibrium constant, it is possible to link the structural parameter of a PCE with its adsorption.[38] We used these analytical expressions to estimate R_g, R_{AC}, S_A, and K_A^* (i.e., $K_A \times 10^5$) for PCE-dispersed portlandite suspensions (see Table 2). Here, we assumed a_N = 0.25 nm, a_P = 0.36 nm, and χ = 0.37 for PEO in water at 25 °C.[33,38] As the length of the side chain increased, the density of the side chain decreased, resulting in the radius of gyration, R_g, of the PCEs not increasing in proportion to the side chain length (see eq 1). Among the three PCEs, the adsorbed layer thickness increases with the length of the side chain. However, it was observed that S_A and K_A^* did not show direct correlations with the length of the side chain. For instance, the estimated adsorption equilibrium constant K_A^* (i.e., $K_A \times 10^5$) is proportional to $\sim N^{7/5}$ and $\sim P^{-9/5}$; thus, the ratio P/N is the dominating factor. Here, PCE 2 showed a higher K_A^*, while PCE 1 and PCE 3 exhibit identical K_A^* values. We note that these equations represent a scaling law that captures the parametric dependencies, though the exactness of the prefactor may be limited.

Table 2. Estimated Radius of Gyration, Adsorbed Layer Thickness, Occupied Surface Area, and Adsorption Equilibrium Constant for the Four PCEs

	radius of gyration, R_g (nm)	radius of hemispheres when adsorbed, R_{AC} (nm)	adsorption equilibrium constant, K_A^* ($K_A \times 10^5$)	surface occupied by each adsorbed molecule, S_A (nm^2)
PCE 1	5.3	3.1	48.4	11,515
PCE 2	4.6	4.4	131.1	10,145
PCE 3	5.7	9.0	43.2	18,270
PCE MG	6.8	6.0	22.2	21,725

Figure 2a shows the adsorption isotherms of different PCEs on portlandite surfaces, represented as the variation in the amount of adsorbed PCEs, ρ_a (i.e., expressed as mass adsorbed per unit surface area of portlandite, mg/m^2), as a function of free PCE in the suspending medium, ρ_f (i.e., expressed in mg/L), for increasing dispersant dosage ρ. Similarly, Figure 2b shows the fractional adsorption of the PCE dispersants, C_a as a function of ρ (note: C_a = 1 − [(amount of PCEs remained nonadsorbed in the suspending medium in mg/L)/(total amount of PCEs added in the suspension in mg/L)]). Here, the shape of the adsorption isotherms allows a qualitative analysis of the adsorption affinity of the PCEs onto a given surface.

All PCEs exhibited similar adsorption (Figure 2a) and fractional adsorption (Figure 2b) profiles. At low dosages, ρ < 0.5 mass %, all PCEs showed a similar extent of adsorption and similar fractional adsorption, ∼80% (Figure 2b). It suggests that only a fixed fraction of the PCE is adsorbed at the beginning, possibly connected to polydispersity in the molecular structure and size of PCEs, as they often contain many fractions of various molecular weights and structures.[26] Importantly, PCEs often have 5−10 mass % of residual side chain monomer, which does not adsorb due to the absence of charged moieties. The initial identical adsorption becomes more differentiated for PCE dosages ρ > 0.5 mass %. Above the initial linear adsorption zone, some PCEs achieve their adsorption saturation limit, while others continue to adsorb slowly with increasing dosages approaching the saturation plateau asymptotically. PCEs with shorter side chains exhibited a marginally higher saturation limit and higher binding affinity (Table 2). The surface area S_A taken up by adsorbed molecules of different PCEs can mostly explain the saturation limit, with the exception of PCE 2, which has a comparable S_A to PCE 1. Largely, the adsorption data suggests that PCEs with larger side chains reach saturation adsorption limits at lower dosages. However, up to a specific dosage, an identical fraction of all PCEs adsorb (i.e., possibly due to their polydispersity) and, subsequently, beyond certain surface coverage, larger PCEs can no longer adsorb while the smaller PCEs continue to adsorb. In addition, the competition between electrostatic attraction and steric repulsion controls the adsorption kinetics of the PCEs and produces noticeable differences in their adsorption behaviors.

We note that the commercial dispersant PCE MG showed a similar adsorption profile as other experimental grade PCEs but exhibited a relatively lower adsorption saturation limit and a higher adsorption affinity corresponding to its side chain length. Evidently, S_A for PCE MG is relatively higher than the others due to its molecular architecture. Additionally, unlike the other three PCEs, PCE MG is a commercial formulation with functional additives, whose presence might lead to their competitive adsorption, which contributes to the differences in its adsorption characteristics. Also, we did not observe a similar trend in the side chain length dependence of adsorption equilibrium constants estimated from the scaling law. It should be taken into account that any cross-validation of the results from the scaling law with experimental adsorption data is subject to the dispersity of the tested PCEs, which affects the prefactors in eqs 1−4.

The PCE dosage levels corresponding to the drop in fractional adsorption from the maximum fractional adsorption plateau, ρ_{opt}^a are denoted by arrows in Figure 2b (see Table 3). PCE adsorption at low dosages (i.e., ρ < 0.5 mass %) is

https://doi.org/10.1021/acs.langmuir.3c00704
Langmuir 2023, 39, 10395−10405

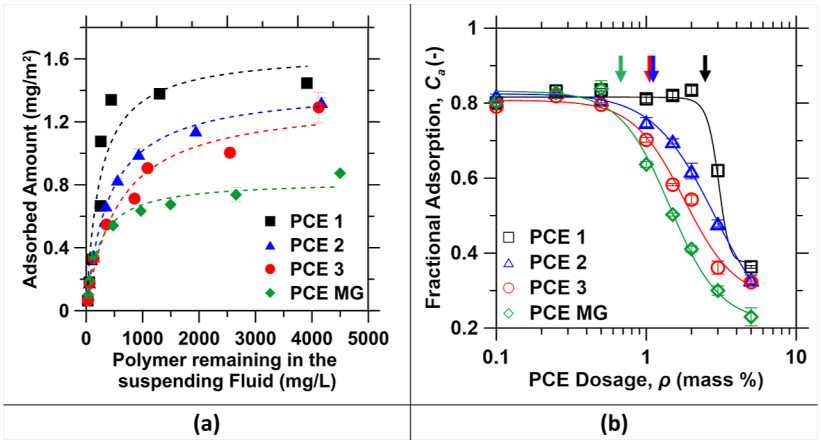

Figure 2. (a) Amount of dispersant adsorbed onto portlandite particle surfaces ρ_a as a function of the concentration of dispersant remaining in the suspending fluid ρ_f. The dashed lines indicate fits to the experimental data and are drawn as a guide for the eye. (b) Variation in the fraction of PCEs adsorbed (C_a) as a function of the PCE dosage ρ. The PCE dosage levels corresponding to the drop in fractional adsorption from the maximum fractional adsorption plateau (i.e., ρ^a_{opt}) are denoted by arrows.

Table 3. Comparison of Optimal PCE Dosages Evaluated from the Adsorption and Rheological Data[**]

	ρ^x_{opt} (mass %)	ρ^y_{opt} (mass %)	ρ^a_{opt} (mass %)
PCE 1	2	2	2.5
PCE 2	1.2	1.3	1.1
PCE 3	1	1	1.05
PCE MG	2	2	0.63

[**]Here, ρ^x_{opt} and ρ^y_{opt} were estimated from the evolutions of the power-law index and yield stress with PCE dosage, respectively, and ρ^a_{opt} was the dosage corresponding to the drop in fractional adsorption from the maximum fractional adsorption plateau.

primarily governed by electrostatics, resulting in identical adsorption behavior since all PCEs possess similar charge densities. With increasing dosage, however, the particle surfaces get increasingly covered by the dispersants, and the steric repulsion between the PEO side chains of the dispersant inhibits further adsorption. This steric repulsion is expected to be stronger for dispersants with longer side chains. Thus, with increasing side chain length, reduced adsorption saturation limits (Figure 2a) and lesser fractional adsorption (at higher dosages) (Figure 2b) of PCEs were observed.

Crucial Attributes of PCEs Influencing the Portlandite Suspension Rheology. Aqueous suspensions of attractive portlandite particles form flocculated fractal networks.[9,10,39] In such suspensions, particle flocculation alters the way shear concentrates between flocs or particles, strongly influencing the apparent viscosity of the suspension.[11,12,40] As the suspensions are subjected to an increasing shear rate $\dot{\gamma}$, the dynamic equilibrium between colloidal interactions and hydrodynamic forces leads to the shear-thinning behavior at low and intermediate $\dot{\gamma}$.[41,42] The shear-induced aggregate breakup, dispersion, and alignment manifest themselves as a decline in the suspension viscosity η, thus producing shear-thinning behavior. Thus, portlandite suspensions exhibited strong shear-thinning flow behavior, as illustrated by the flow curves for a portlandite suspension with $\phi = 0.3$ (Figure 3a).

Tuning the colloidal interparticle forces can enable modulation of the flow characteristics of portlandite suspensions. Adsorption of PCEs provides steric stabilization that moderates the magnitude of the interparticle attractive Van der Waals forces between particles, manifesting a reduction in the yield stress of suspensions.[19,33] The adsorbed PCEs also change the flocculation state by progressively breaking down the particulate aggregates, which modifies the way shear concentrates and localizes in the liquid layers between flocs, leading to a reduction in plastic viscosity.[40,43] Thus, PCE dispersants can "soften" the shear thinning behavior, as is evident in the flow curves for $\phi = 0.3$ portlandite suspensions with increasing dosage ρ of PCE 2, shown in Figure 3a. Subsequently, an optimal dosage, ρ_{opt} was noted for each PCE, wherein the suspensions undergo a transition from a shear-thinning flow behavior to a nearly Newtonian flow response (i.e., η being independent of $\dot{\gamma}$) (Figure 3a,b). Thus, the optimal dosage induces an improved and dynamically equilibrated dispersion state of portlandite particle aggregates. Further, the evolution of shear stress with $\dot{\gamma}$ (Figure 3b) revealed a transition from a yield stress fluid with multiple yielding events to a nearly Newtonian fluid with substantially subdued yield with increasing ρ.

Similar transitions in flow behavior (i.e., from multiple yielding events to single step yielding) with the increase in PCE dosage were observed in dynamic strain sweeps of portlandite suspensions (Figure 3c; note: neat and PCE dosed suspensions with identical yield stress were selected here for the demonstration). Neat portlandite suspensions exhibit a two-stage yielding behavior typical of attractive colloidal suspensions.[44−48] For all four PCEs, portlandite suspensions approached a single-step yielding with increasing PCE dosage and subsequently exhibited a substantially subdued yielding, typical of systems with repulsive or weak interactions.[49] Often, colloidal systems that feature structure over two-length scales tend to exhibit two-step yielding.[49] The two-step yielding phenomenon can be linked to the heterogeneity in the form of particle aggregates and percolated clusters (i.e., the network structure formed via. interconnected particle aggregates), constituting two different length scales in colloidal systems.[49] The first yielding corresponds to the rupturing of inter-cluster bonds in the percolated network, while the subsequent yielding is linked to the breaking of individual particle agglomerates. The same kind of bonds are broken on a particle level in the first and second yielding processes; however, on a mesoscopic scale, they are intracluster bonds (i.e., connecting individual

https://doi.org/10.1021/acs.langmuir.3c00704
Langmuir 2023, 39, 10395−10405

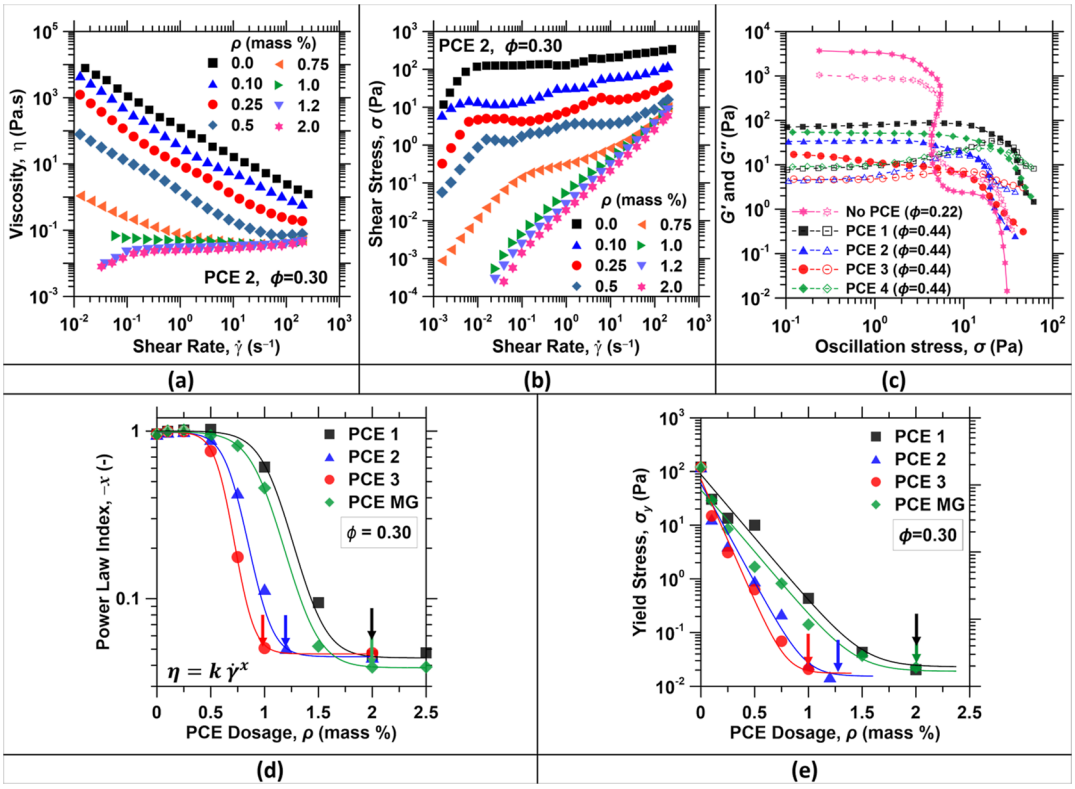

Figure 3. (a,b) Set of representative flow curves showing the shear-thinning to Newtonian-like transition in the flow behavior of portlandite suspensions (ϕ = 0.30) with increasing PCE 2 dosage. The shear-rate sweep experiments were repeated three times, yielding an uncertainty in the determined apparent viscosity values <12%; (c) dynamic strain sweeps of neat and optimally dosed portlandite suspensions with matching yield stress at ω = 0.5 Hz. The dynamic moduli are plotted herein as a function of measured stress; (d) variation in the power-law index x of the flow curves as a function of dosage for different PCE dispersants; (e) variation in the yield stress σ_y of suspensions as a function of dosage for different PCE dispersants. [Note: (i) estimation of σ_y and x from the flow curves is illustrated in Figure S2a,b in the Supporting Information. Arrows in (d,e) denote the optimal dosages estimated from sigmoidal fits applied to the x and σ_y evolutions. The details of the sigmoidal fits are provided in Figure S2c in the Supporting Information. A few suspensions with a higher PCE dosage showed no signs of even subdued yield, their yield stress was assumed to be zero, and these were excluded from the results shown in Figure 3e].

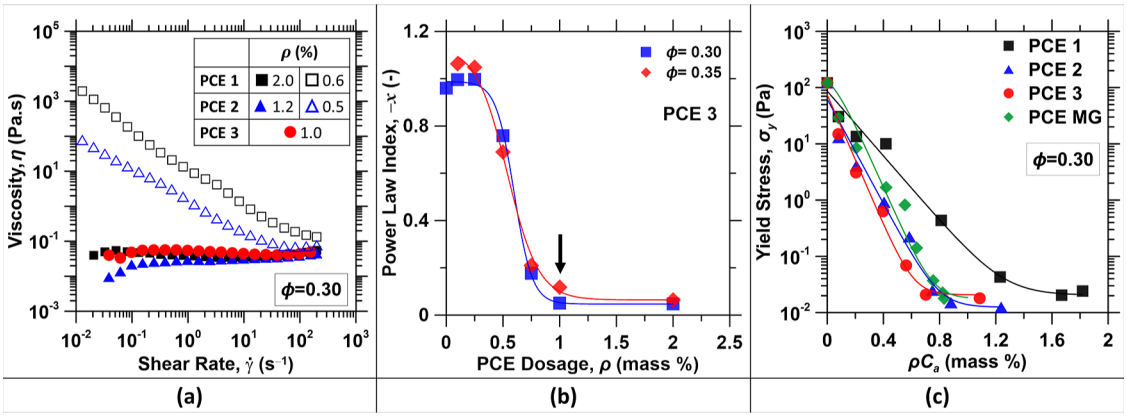

Figure 4. (a) Flow curves of suspensions (ϕ = 0.30) containing different PCEs with their dosage adjusted to (i) optimal dosage (i.e., ρ^{x}_{opt}) and (ii) identical total anionic charge units; (b) variation in the power-law index, x of the flow curves of PCE 3 dosed portlandite suspensions with ϕ = 0.30 and ϕ = 0.35. The arrow denotes the optimal dosage estimated from sigmoidal fits applied to the evolutions of the power law index with PCE dosage; (c) variation in the yield stress σ_y of suspensions (ϕ = 0.30) as a function of adsorbed dosage (i.e., $\rho \times C_a$) of PCEs. Sigmoidal fits are applied to the power-law index and the yield stress data to extract the optimal PCE dosage.

particles in a cluster) and intercluster bonds (i.e., connecting individual clusters), respectively.[50]

The modulation of the flow characteristics of portlandite suspensions by PCE dispersants can be summarized by analyzing the dependence of the shear-thinning index x and yield stress σ_y on PCE dispersant type and dosage (Figure 3d,e). At very low PCE dosages, x is close to 1, and corresponding σ_y is of the order 10^1 to 10^2 Pa. Increasing ρ decreases x and σ_y (Figure 3d,e), wherein x tends to 0 and σ_y decreases by 3−4 orders of magnitude. Beyond the optimal PCE dosage, ρ_{opt}, the suspensions demonstrated Newtonian-like rheological response with $x \sim 0$, and σ_y tends zero with an

https://doi.org/10.1021/acs.langmuir.3c00704
Langmuir 2023, 39, 10395−10405

increase in ρ. Notably, some of the suspensions with particularly high dosages of PCE did not show any signs of yielding, and as such, their yield stress was taken to be zero and were not included in Figure 3e.

Sigmoidal fits were applied to the x and σ_y evolutions to estimate the optimal PCE dosage for rheology modification. Table 3 compares the optimal PCE dosage obtained from adsorption measurements (ρ^a_{opt}, Figure 2b) with the optimal dosages estimated from x and σ_y evolutions, ρ^x_{opt} and ρ^y_{opt}, respectively (denoted by arrows in Figure 3d,e). The optimal dosages ρ^x_{opt} and ρ^y_{opt} were expectedly found to be in close agreement with each other for each of the PCEs and exhibited a non-trivial correlation with ρ^a_{opt}. Comparing the adsorption characteristics of PCEs on portlandite particles with the rheology modifications in portlandite suspensions is noteworthy. For PCEs with longer side chain lengths, despite a lower fraction being adsorbed onto the portlandite surface (see Figure 1), the σ_y and x evolutions exhibited a stronger dependence on PCE dosage. We note that the x and σ_y evolutions of PCE MG are not in line with this trend, likely due to its relatively lower adsorption onto the portlandite surfaces. Notably, the modifications in portlandite suspension rheology with increasing dispersant dosage essentially follow a similar trend across all PCEs (i.e., manifested in x and σ_y evolutions, Figure 3d,e). The extent of adsorption of PCE on portlandite particles and the maximum adsorption limit are governed by the available solid surface area, the PCE backbone charge density, and the PCE side chain length. The suspension rheology and optimal dosage, in addition to being controlled by the extent of adsorption, are also dictated by adsorbed layer thickness,[9] which, in turn, often grows with increasing side chain length.

As such, suspensions containing an optimal dosage of different PCEs (i.e., ρ^x_{opt}) exhibit identical flow behavior (Figure 4a). When the PCE dosage was adjusted to achieve equivalent total anionic charge units in suspensions (i.e., ρ for each PCE was adjusted according to its charge density and molecular weight to match the total number of anionic units in the suspensions), it was apparent that PCE 3 significantly reduced the yield stress and viscosity when compared to PCE 1 and PCE 2 (Figure 4a). Further, the optimum dosage remained essentially the same across different ϕ (Figure 4b). When the PCE dosage was normalized with respect to their fractional adsorption to eliminate the effect of the extent of adsorption, the role of side chain length in controlling the portlandite aggregation became apparent (Figure 4c). It is evident that a smaller fraction of adsorbed PCE with a longer side chain length is required to achieve the targeted reductions in yield stress and viscosity. Thus, although a lower extent of adsorption is achieved for PCEs with longer side chain lengths, the superior steric hindrance (i.e., longer-range geometrical particle−particle exclusion steric hindrance) makes them a more effective dispersant.

Aggregation, Jamming, and Yielding of PCE-Dosed Portlandite Suspensions. Several engineering applications involving particulate suspensions require maximizing particle loading as close as possible to the maximum permissible particle loadings ϕ_m while ensuring flowability and processability. For portlandite suspensions, yield stress and viscosity diverge at a critical volume fraction $\phi_m \sim 0.35$ (see Figure S3 in the Supporting Information) that is far lower than the maximum packing fraction for random close packing of monosized spheres (i.e., $\phi_0 = 0.64$), owing to significant particle aggregation and non-spherical shape particles, especially particles with extended aspect ratios.[9,10] PCEs modulate the interparticle interactions and particle aggregation state, altering their jamming and yielding characteristics and increasing suspension ϕ_m.[46,49,51] Figure 5 illustrates the evolution of σ_y

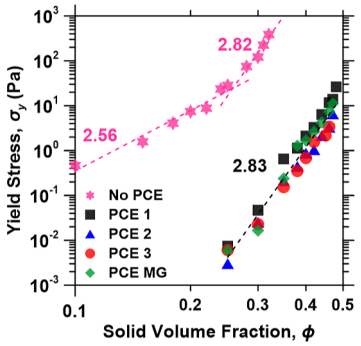

Figure 5. Yield stress of neat and PCE-dosed (i.e., optimally dosed) portlandite suspensions as a function of solid volume fraction ϕ. The coefficient of variation from three yield stress data replicates was <15%. The dashed lines present the power-law scaling, $\sigma_y \propto \phi^C$ with the corresponding fractal dimensions estimated by the power-law exponent, C noted next to each. The maximum estimated uncertainty in the d_f calculations is ±0.03. (Note: the yield stress was measured for suspensions at $\phi < \phi_{max}$ (i.e., upto 0.34 for neat suspensions and up to 0.47 for suspensions with PCE).

with solid volume fraction (ϕ) for neat (i.e., $\rho = 0$) and optimally dosed (i.e., containing an optimal dosage $\rho = \rho^x_{opt}$) portlandite suspensions. The neat portlandite suspensions presented a power-law behavior ($\sigma_y \propto \phi^C$) featuring two distinct dependencies on ϕ with distinct power-law exponents. As such, above a transition volume fraction ϕ_T, σ_y displayed a stronger reliance on ϕ.[10] In contrast, PCE-dosed suspensions exhibited a single $\sigma_y \propto \phi^C$ power law dependence across the entire ϕ range. Further, PCE dispersants improved ϕ_m of the suspensions, and the improvements were largely independent of the side chain length of PCEs (see Figure S3 in the Supporting Information). Importantly, $\sigma_y - \phi$ data corresponding to different PCE-dosed suspensions were effectively collapsed onto a single master curve, suggesting functionally similar microstructures and aggregate networks in all the PCE-dosed suspensions (Figure 5). Thus, when compared at optimal dosage and hence the analogous flocculation state, the side chain length of the PCEs does not significantly affect the microstructural evolution in these suspensions.

Using the fractal elasticity model, a connection can be established between the scaling exponent C and the fractal dimension of the flocs d_f as: $C = (d - 1)/(d - d_f)$, where d denotes the Euclidean dimension (e.g., $d = 3$ for three-dimensional setting).[52−54] The switch in the power-law behavior of neat portlandite suspensions is believed to be caused by a change from strong-link to weak-link behavior among the flocs when ϕ increases.[54] At low ϕ values, the fractal elasticity model presumes a strong-link behavior, resulting from inter-floc links being stronger than intra-floc links. Subsequently, as ϕ is increased, the flocs become smaller and tougher because of the crowding of the particles, and the suspensions may enter a weak-link domain where the intra-floc bonds become stronger than those between flocs.[52] As a result, the macroscopic rheological attributes of a suspension (i.e., elastic and yielding characteristics) depend largely on how its

https://doi.org/10.1021/acs.langmuir.3c00704
Langmuir 2023, 39, 10395−10405

intra-floc links beak down in the strong-link regime and its inter-floc links fail in the weak-link regime.[10] PCE dosed suspensions did not exhibit a strong-link to weak-link transition and possessed a similar fractal dimension d_f when compared to neat suspensions in the weak-link regime ($d_{f,neat}$ = 2.56 ($\phi < \phi_T$), 2.82 ($\phi > \phi_T$), and $d_{f,PCE}$ = 2.83). A lower d_f value suggests a more open fractal network structure in the suspensions,[55] while a larger d_f value is indicative of the more compact and denser structure of the flocs.[56] For the PCE dosed suspensions, $d_{f,PCE}$ = 2.83 suggests that the flocs are relatively small, possibly with a width of a few particle diameters, regardless of the ϕ. It is remarkable that despite exhibiting distinct yield stress behavior, neat portlandite suspensions (for $\phi > \phi_T$) and PCE doped suspensions still demonstrate a similar $\sigma_y - \phi$ power-law relationship (i.e., identical C and d_f). This can be attributed to the fact that, at such dense concentrations, the suspension elasticity is determined by glassy features rather than the fractal elasticity model.[57] As ϕ goes up further in the weak-link domain, the flocs become more tightly packed and the weak inter-floc connections become less evident. In these cases, the geometric resistance caused by the crowding of the aggregate becomes more dominant than the weak inter-floc links.[58] A considerable geometric resistance encountered necessitates extra energy to separate the aggregates apart from each other, in addition to that necessary to break the inter-floc and intra-floc bonds.[58,59] The PCE dosed suspensions displayed a substantially lower σ_y than the pure portlandite suspensions across the studied ϕ values. This could be due to the effect of PCE-induced steric stabilization, which reduces the number of aggregates present or decreases the number of cluster−cluster bonds, thereby leading to a decrease in yield stresses.

In addition, despite differences in the adsorbed layer thickness and the surface area occupied, PCE-dosed suspensions with an optimal dosage still showed an identical $\sigma_y - \phi$ power-law relationship. It is worth noting that, with increasing side chain lengths of PCEs, the adsorbed layer thickness increases while the adsorption saturation limit and optimal dosage decrease. Despite the lower adsorption saturation limit and fractional adsorption, the higher steric hindrance caused by longer side chain PCEs contributes to better limiting particle aggregation even at low dosages. Nevertheless, when dosed at optimal dosages, different PCE-dosed portlandite suspensions exhibit identical microstructural evolution and fractal structuring and, therefore, demonstrate a similar $\sigma_y - \phi$ power-law relationship, regardless of the side chain length, as schematically illustrated in Figure 6. Notably, at the optimal dose, thus in a comparable flocculation state, the side chain length of the PCEs does not significantly influence the microstructural development in these suspensions.

Mitigation of Temperature-Induced Aggregation by PCEs. The diminution of electrostatic repulsive interparticle interactions with increasing temperature enhances particle aggregation and can induce an anomalous increase in a suspension's viscosity.[10] These temperature-induced alterations in rheology can impact a suspension's processability.[60] Here, the rheological responses of PCE-dosed portlandite suspensions were probed at varied temperatures to investigate the thermal response of PCE-induced stabilization of suspension rheology (Figure 7). Optimally dosed suspensions (i.e., $\rho = \rho^x_{opt}$ estimated for 25 °C) exhibited an increase in viscosity with an increase in temperature (i.e., represented by an unphysical "negative" activation energy, E_a), suggesting

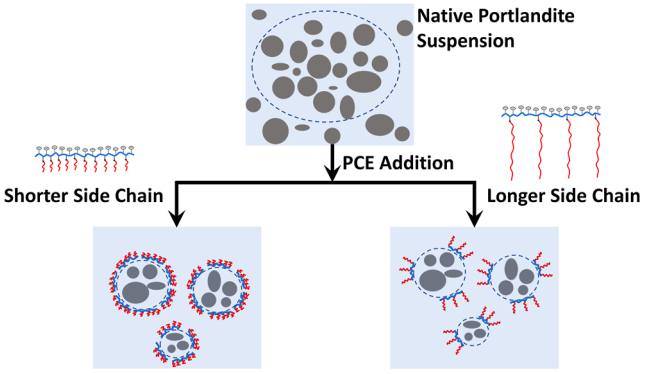

Figure 6. Schematic illustrating the deflocculation mechanism in portlandite suspensions containing PCE of different side chain lengths. With increasing side chain length of PCEs, the adsorbed layer thickness increases while the adsorption saturation limit and optimal dosage decrease. The longer side-chain PCEs are more effective in affecting suspension viscosity and yield stress in spite of their lower adsorption saturation limit and fractional adsorption. The superior steric hindrance induced by the longer side chain PCEs results in better efficacy in mitigating particle aggregation even at low dosages. However, when dosed at optimal dosages, different PCE-dosed portlandite suspensions exhibit identical microstructural evolution and fractal structuring, and hence, exhibit a similar $\sigma_y - \phi$ power-law relationship, regardless of the side chain length. The flocculation state of the suspensions, as indicated by $d_{f,PCE}$ = 2.83, indicates that the flocs are relatively small, possibly with a width of a few particle diameters.

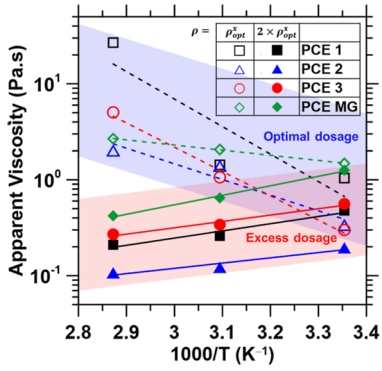

Figure 7. Arrhenius plots of apparent viscosity (η, measured at $\dot{\gamma}$ = 1 s^{-1}) for portlandite suspensions (ϕ = 0.4 at $\dot{\gamma}$ = 1 s^{-1}) dosed with an optimal ($\rho = \rho^x_{opt}$) and excess ($\rho = 2\rho^x_{opt}$) amount of PCEs. The data were fitted using an Arrhenius-like equation, $\eta = \eta_\infty \exp(E_a/RT)$ with η_∞, R, E_a, and T being the exponential prefactor, gas constant, apparent activation energy, and thermodynamic temperature, respectively.[61] Table S1 in the Supporting Information lists the estimated E_a values for PCE dosed suspensions. The green and blue shades in the plot are provided to illustrate the distinct temperature-dependent rheological responses of optimal and excess PCE-dosed suspensions. An uncertainty of ≤15% was observed in the apparent viscosity data based on three replicate measurements.

temperature-induced particle aggregation. In contrast, suspensions with an excess PCE dosage (i.e., $\rho = 2\rho^x_{opt}$) exhibited a moderate reduction in their apparent viscosity when increasing the temperature (i.e., positive E_a, especially at high shear rates), suggesting an improved dispersion state of portlandite particulates in these suspensions.

The coupling between temperature-induced aggregation and the PCE dosage in electrosterically stabilized portlandite suspensions indicates that temperature significantly affects

https://doi.org/10.1021/acs.langmuir.3c00704
Langmuir 2023, 39, 10395−10405

PCE adsorption on the surfaces of portlandite particulates. The adsorption of PCEs is often known to increase with temperature, increasing the adsorption saturation limit.[62−64] Thus, an optimally dosed suspension at room temperature may become undersaturated at higher temperatures, requiring additional PCE molecules to reach a new equilibrium level of adsorption.[64] Thus, these suspensions with insufficient PCE dosage and empty surface-active sites induce bridging attraction and flocculation, presenting an increasing viscosity with temperature. In contrast, when there is excess PCE in the suspension, the enhanced adsorption at elevated temperatures would lead to a rise in the total energy barrier for particle aggregation, resulting in an improved dispersion state of particles and a reduction in suspension viscosity. Notably, all four PCEs exhibited similar trends in the temperature-dependent rheology of portlandite suspensions. We note that comprehensive adsorption studies at different temperatures are essential to gain further insights into the role of side chain length in controlling the temperature-dependent PCE confirmation and adsorption characteristics onto portlandite surfaces. Nevertheless, it is obvious that the temperature-dependent rheology of portlandite suspensions can be tailored by adjusting the PCE dosage to meet the specific processing requirements of the engineering application.

CONCLUSIONS

This study defines the correlations between the PCE characteristics and the macroscopic rheological characteristics of portlandite suspensions. PCEs with longer side chains show lower fractional adsorption and adsorption saturation limits due to higher steric repulsion from the PCE chains that are already adsorbed on the particle surfaces. However, the longer side chain PCEs induced a transition from a strong shear-thinning to a nearly Newtonian flow behavior with substantially subdued yielding at lower dosages, suggesting their better efficacy in mitigating particle aggregation. Thus, the longer side chain PCEs were more effective in moderating the viscosity and yield stress of portlandite suspensions, despite offering lower surface coverage. The superior steric hindrance (i.e., longer-range geometrical particle−particle exclusion steric hindrance) introduced by the longer-side chain PCEs makes them a more effective dispersant than the shorter-side chain counterparts.

Regardless of the side chain length, PCE-dosed portlandite suspensions exhibit identical yield stress and apparent viscosity when dosed at the optimum dosage (i.e., a dosage that induces a dynamically equilibrated dispersion state of portlandite particle aggregates). Optimally dosed portlandite suspensions exhibit an equivalent maximum achievable volume fraction ϕ_m, a single power law dependence across the entire ϕ range, and an identical fractal dimension, pointing towards a similar fractal structuring and flocculation state in the PCE-dosed suspensions. On the other hand, the neat portlandite suspensions exhibited a two-step yielding (as opposed to a single-step yielding in PCE-dosed suspensions), suggesting the transition from an attractive to repulsive gel transition in PCE-dosed suspensions with optimal dosing. Furthermore, the temperature-dependent rheological responses of portlandite suspensions can be tailored by adjusting the PCE dosage. Optimally dosed suspensions did not change the temperature-induced aggregation, while excess PCE dosing did due to increased PCE adsorption at higher temperatures. Thus, excess PCE dosing in portlandite suspensions can effectively mitigate temperature-induced aggregation and the consequent increase in suspension viscosity.

The outcomes of this work provide key insights for controlling and tailoring the rheology of portlandite suspensions across different processing conditions. These essential understandings can be extended in general to a wide range of colloidal suspensions with high ionic strength and strong charge screening behavior, providing valuable guidance for choosing an efficient dispersant and its dosage for an array of engineering applications.

ASSOCIATED CONTENT

Supporting Information

The Supporting Information is available free of charge at https://pubs.acs.org/doi/10.1021/acs.langmuir.3c00704.

Particle size distribution of commercial portlandite powder obtained using static light scattering, scanning electron microscopy images of portlandite particulates, flow curves of portlandite suspensions illustrating the procedures used to calculate the shear-thinning index (x), yield stress (σ_y), and optimal yield stress (ρ^x_{opt}), yield stress evolution of neat and PCE-dosed portlandite suspensions as a function of solid volume fraction ϕ illustrating ϕ_m, estimated apparent activation energy, and E_a values for the PCE-dosed suspensions for different PCE dosing (PDF)

AUTHOR INFORMATION

Corresponding Authors

Sharu Bhagavathi Kandy − *Laboratory for the Chemistry of Construction Materials (LC²), Department of Civil and Environmental Engineering and Institute for Carbon Management (ICM), University of California, Los Angeles, California 90095, United States;* orcid.org/0000-0001-9939-8239; Email: bksharu@gmail.com, sharubk@nitc.ac.in

Gaurav Sant − *Laboratory for the Chemistry of Construction Materials (LC²), Department of Civil and Environmental Engineering, Institute for Carbon Management (ICM), California Nanosystems Institute (CNSI), and Department of Materials Science and Engineering, University of California, Los Angeles, California 90095, United States;* orcid.org/0000-0002-1124-5498; Email: gsant@ucla.edu

Authors

Narayanan Neithalath − *School of Sustainable Engineering and the Built Environment, Arizona State University, Tempe, Arizona 86587, United States*

Mathieu Bauchy − *Institute for Carbon Management (ICM) and Laboratory for the Physics of AmoRphous and Inorganic Solids (PARISlab), Department of Civil and Environmental Engineering, University of California, Los Angeles, California 90095, United States;* orcid.org/0000-0003-4600-0631

Aditya Kumar − *Department of Materials Science and Engineering, Missouri University of Science and Technology, Rolla, Missouri 65409, United States;* orcid.org/0000-0001-7550-8034

Edward Garboczi − *Applied Chemicals and Materials Division, Material Measurement Laboratory, National Institute of Standards and Technology, Boulder, Colorado 80305, United States*

https://doi.org/10.1021/acs.langmuir.3c00704
Langmuir 2023, 39, 10395−10405

Torben Gaedt − *Department of Chemistry, Technische Universität München, Garching bei München D-85747, Germany*

Samanvaya Srivastava − *Institute for Carbon Management (ICM), Department of Chemical and Biomolecular Engineering, UCLA Center for Biological Physics, and California Nanosystems Institute (CNSI), University of California, Los Angeles, California 90095, United States;* orcid.org/0000-0002-3519-7224

Complete contact information is available at: https://pubs.acs.org/10.1021/acs.langmuir.3c00704

Notes

The authors declare no competing financial interest.

■ ACKNOWLEDGMENTS

The authors gratefully acknowledge the financial support for this research from the U.S. National Science Foundation (DMREF: 1922167), TRANSCEND, a joint UCLA-NIST Consortium that is funded by its industry and agency partners, Bavaria-California Technology Center (BaCaTec), The Advanced Research Projects Agency-Energy (ARPA-e: DE-AR-0001147), and the 3DConcrete Printing Network for Accelerating Progress in Concrete Manufacturing supported by the U.S. National Science Foundation (AccelNet OISE: 2020095). This research was conducted in the Laboratory for the Chemistry of Construction Materials (LC^2) and UCLA's Electron Microscopy Core Facility. The authors express their gratitude to the laboratories that have supported and enabled this research. The contents of this paper reflect the views and opinions of the authors, who are responsible for the accuracy of the datasets presented herein, and do not reflect the views and/or policies of the funding agencies, nor do the contents constitute a specification, standard, or regulation.

■ ADDITIONAL NOTE

[a]Certain commercial equipment, software, and/or materials are identified in this paper in order to adequately specify the experimental procedure. In no case does such identification imply recommendation or endorsement by the National Institute of Standards and Technology, nor does it imply that the equipment and/or materials used are necessarily the best available for the purpose.

■ REFERENCES

(1) Martínez-Bustos, F.; Chang, Y. K.; Bannwart, A. C.; Rodríguez, M. E.; Guedes, P. A.; Gaiotti, E. R. Effects of Calcium Hydroxide and Processing Conditions on Corn Meal Extrudates. *Cereal Chem.* **1998**, *75*, 796−801.

(2) Adroer, M.; Valero, F.; Poch, M.; Solà, C. A New Procedure for Water Decarbonation Process Control. *Ind. Eng. Chem. Res.* **1994**, *33*, 1501−1509.

(3) Lim, S.; Jeon, W.; Lee, J.; Lee, K.; Kim, N. Engineering Properties of Water/Wastewater-Treatment Sludge Modified by Hydrated Lime, Fly Ash and Loess. *Water Res.* **2002**, *36*, 4177−4184.

(4) Elert, K.; Rodriguez-Navarro, C.; Pardo, E. S.; Hansen, E.; Cazalla, O. Lime Mortars for the Conservation of Historic Buildings. *Stud. Conserv.* **2002**, *47*, 62−75.

(5) Rodriguez-Navarro, C.; Suzuki, A.; Ruiz-Agudo, E. Alcohol Dispersions of Calcium Hydroxide Nanoparticles for Stone Conservation. *Langmuir* **2013**, *29*, 11457−11470.

(6) Falzone, G.; Mehdipour, I.; Neithalath, N.; Bauchy, M.; Simonetti, D.; Sant, G. New Insights into the Mechanisms of Carbon Dioxide Mineralization by Portlandite. *AIChE J.* **2021**, *67*, No. e17160.

(7) Sant, G.; Mehdipour, I.; Falzone, G. D. Formulations and Processing of Cementitious Components to Meet Target Strength and CO2 Uptake Criteria. U.S. patent 0,299,203 A1, 2020.

(8) Murray, P. E.; Hafez, A. A.; Smith, A. J.; Cox, C. F. Hierarchy of Pulp Capping and Repair Activities Responsible for Dentin Bridge Formation. *Am. J. Dent.* **2002**, *15*, 236−243.

(9) Timmons, J.; Mehdipour, I.; Gao, S.; Atahan, H.; Neithalath, N.; Bauchy, M.; Garboczi, E.; Srivastava, S.; Sant, G. Dispersing Nano- and Micro-Sized Portlandite Particulates via Electrosteric Exclusion at Short Screening Lengths. *Soft Matter* **2020**, *16*, 3425−3435.

(10) Bhagavathi Kandy, S.; Mehdipour, I.; Neithalath, N.; Bauchy, M.; Garboczi, E.; Srivastava, S.; Gaedt, T.; Sant, G. Temperature-Induced Aggregation in Portlandite Suspensions. *Langmuir* **2020**, *36*, 10811−10821.

(11) Fourmentin, M.; Ovarlez, G.; Faure, P.; Peter, U.; Lesueur, D.; Daviller, D.; Coussot, P. Rheology of Lime Paste—a Comparison with Cement Paste. *Rheol. Acta* **2015**, *54*, 647−656.

(12) Ruiz-Agudo, E.; Rodriguez-Navarro, C. Microstructure and Rheology of Lime Putty. *Langmuir* **2010**, *26*, 3868−3877.

(13) Russel, W. B.; Saville, D. A.; Schowalter, W. R. *Colloidal Dispersions*; Cambridge University Press, 1991.

(14) Srivastava, S.; Shin, J. H.; Archer, L. A. Structure and Rheology of Nanoparticle-Polymer Suspensions. *Soft Matter* **2012**, *8*, 4097−4108.

(15) Kamiya, H.; Fukuda, Y.; Suzuki, Y.; Tsukada, M.; Kakui, T.; Naito, M. Effect of Polymer Dispersant Structure on Electrosteric Interaction and Dense Alumina Suspension Behavior. *J. Am. Ceram. Soc.* **2004**, *82*, 3407−3412.

(16) Rhodes, S. K.; Lambeth, R. H.; Gonzales, J.; Moore, J. S.; Lewis, J. A. Cationic Comb Polymer Superdispersants for Colloidal Silica Suspensions. *Langmuir* **2009**, *25*, 6787−6792.

(17) Kirby, G. H.; Lewis, J. A. Comb Polymer Architecture Effects on the Rheological Property Evolution of Concentrated Cement Suspensions. *J. Am. Ceram. Soc.* **2004**, *87*, 1643−1652.

(18) Klimkevicius, V.; Graule, T.; Makuska, R. Effect of Structure of Cationic Comb Copolymers on Their Adsorption and Stabilization of Titania Nanoparticles. *Langmuir* **2015**, *31*, 2074−2083.

(19) Houst, Y. F.; Bowen, P.; Perche, F.; Kauppi, A.; Borget, P.; Galmiche, L.; Le Meins, J. F.; Lafuma, F.; Flatt, R. J.; Schober, I.; Banfill, P. F. G.; Swift, D. S.; Myrvold, B. O.; Petersen, B. G.; Reknes, K. Design and Function of Novel Superplasticizers for More Durable High Performance Concrete (Superplast Project). *Cem. Concr. Res.* **2008**, *38*, 1197−1209.

(20) Ferrari, L.; Kaufmann, J.; Winnefeld, F.; Plank, J. Multi-Method Approach to Study Influence of Superplasticizers on Cement Suspensions. *Cem. Concr. Res.* **2011**, *41*, 1058−1066.

(21) Plank, J.; Pöllmann, K.; Zouaoui, N.; Andres, P. R.; Schaefer, C. Synthesis and Performance of Methacrylic Ester Based Polycarboxylate Superplasticizers Possessing Hydroxy Terminated Poly (Ethylene Glycol) Side Chains. *Cement Concr. Res.* **2008**, *38*, 1210−1216.

(22) Jolicoeur, C.; Simard, M. Chemical Admixture-Cement Interactions : Phenomenology and Physico-Chemical Concepts. *Cem. Concr. Res.* **1998**, *20*, 87−101.

(23) Uchikawa, H.; Hanehara, S.; Sawaki, D. The Role of Steric Repulsive Force in the Dispersion of Cement Particles in Fresh Paste Prepared with Organic Admixture. *Cem. Concr. Res.* **1997**, *27*, 37−50.

(24) Kang, S. H.; Kwon, M.; Kwon, Y. H.; Moon, J. Effects of Polycarboxylate Ether (PCE)-Based Superplasticizer on the Dissolution and Subsequent Hydration of Calcium Oxide (CaO). *Cem. Concr. Res.* **2021**, *146*, 106467.

(25) Gay, C.; Raphaël, E. Comb-like Polymers inside Nanoscale Pores. *Adv. Colloid Interface Sci.* **2001**, *94*, 229−236.

(26) Aïtcin, P. C.; Flatt, R. J. *Science and Technology of Concrete Admixtures*; Civil and Structural Engineering; Woodhead Publishing, 2015.

(27) Yoshioka, K.; Tazawa, E. I.; Kawai, K.; Enohata, T. Adsorption Characteristics of Superplasticizers on Cement Component Minerals. *Cem. Concr. Res.* **2002**, *32*, 1507−1513.
(28) Zingg, A.; Winnefeld, F.; Holzer, L.; Pakusch, J.; Becker, S.; Gauckler, L. Adsorption of Polyelectrolytes and Its Influence on the Rheology, Zeta Potential, and Microstructure of Various Cement and Hydrate Phases. *J. Colloid Interface Sci.* **2008**, *323*, 301−312.
(29) Papo, A.; Piani, L. Effect of Various Superplasticizers on the Rheological Properties of Portland Cement Pastes. *Cem. Concr. Res.* **2004**, *34*, 2097−2101.
(30) Yamada, K.; Takahashi, T.; Hanehara, S.; Matsuhisa, M. Effects of the Chemical Structure on the Properties of Polycarboxylate-Type Superplasticizer. *Cem. Concr. Res.* **2000**, *30*, 197−207.
(31) Winnefeld, F.; Becker, S.; Pakusch, J.; Götz, T. Effects of the Molecular Architecture of Comb-Shaped Superplasticizers on Their Performance in Cementitious Systems. *Cem. Concr. Compos.* **2007**, *29*, 251−262.
(32) Kunhi Mohamed, A.; Weckwerth, S. A.; Mishra, R. K.; Heinz, H.; Flatt, R. J. Molecular Modeling of Chemical Admixtures; Opportunities and Challenges. *Cem. Concr. Res.* **2022**, *156*, 106783.
(33) Flatt, R. J.; Schober, I.; Raphael, E.; Plassard, C.; Lesniewska, E. Conformation of Adsorbed Comb Copolymer Dispersants. *Langmuir* **2009**, *25*, 845−855.
(34) Borget, P.; Galmiche, L.; Le Meins, J. F.; Lafuma, F. Microstructural Characterisation and Behaviour in Different Salt Solutions of Sodium Polymethacrylate-g-PEO Comb Copolymers. *Colloids Surf., A* **2005**, *260*, 173−182.
(35) Kauppi, A.; Andersson, K. M.; Bergström, L. Probing the Effect of Superplasticizer Adsorption on the Surface Forces Using the Colloidal Probe AFM Technique. *Cem. Concr. Res.* **2005**, *35*, 133−140.
(36) Caruso, F.; Mantellato, S.; Palacios, M.; Flatt, R. J. ICP-OES Method for the Characterization of Cement Pore Solutions and Their Modification by Polycarboxylate-Based Superplasticizers. *Cem. Concr. Res.* **2017**, *91*, 52−60.
(37) Giraudeau, C.; D'Espinose De Lacaillerie, J. B.; Souguir, Z.; Nonat, A.; Flatt, R. J. Surface and Intercalation Chemistry of Polycarboxylate Copolymers in Cementitious Systems. *J. Am. Ceram. Soc.* **2009**, *92*, 2471−2488.
(38) Marchon, D.; Sulser, U.; Eberhardt, A.; Flatt, R. J. Molecular Design of Comb-Shaped Polycarboxylate Dispersants for Environmentally Friendly Concrete. *Soft Matter* **2013**, *9*, 10719−10728.
(39) Flatt, R. J.; Bowen, P. Yodel: A Yield Stress Model for Suspensions. *J. Am. Ceram. Soc.* **2006**, *89*, 1244−1256.
(40) Hot, J.; Bessaies-Bey, H.; Brumaud, C.; Duc, M.; Castella, C.; Roussel, N. Adsorbing Polymers and Viscosity of Cement Pastes. *Cem. Concr. Res.* **2014**, *63*, 12−19.
(41) Roussel, N.; Lemaître, A.; Flatt, R. J.; Coussot, P. Steady State Flow of Cement Suspensions: A Micromechanical State of the Art. *Cem. Concr. Res.* **2010**, *40*, 77−84.
(42) Brady, J. F.; Vicic, M. Normal Stresses in Colloidal Dispersions. *J. Rheol.* **1995**, *39*, 545−566.
(43) Bey, H. B.; Hot, J.; Baumann, R.; Roussel, N. Consequences of Competitive Adsorption between Polymers on the Rheological Behaviour of Cement Pastes. *Cem. Concr. Compos.* **2014**, *54*, 17−20.
(44) Mohraz, A.; Solomon, M. J. Orientation and Rupture of Fractal Colloidal Gels during Start-up of Steady Shear Flow. *J. Rheol.* **2005**, *49*, 657−681.
(45) Derec, C.; Ducouret, G.; Ajdari, A.; Lequeux, F. Aging and Nonlinear Rheology in Suspensions of Polyethylene Oxide−Protected Silica Particles. *Phys. Rev. E: Stat. Phys., Plasmas, Fluids, Relat. Interdiscip. Top.* **2003**, *67*, 061403.
(46) Koumakis, N.; Petekidis, G. Two Step Yielding in Attractive Colloids: Transition from Gels to Attractive Glasses. *Soft Matter* **2011**, *7*, 2456−2470.
(47) Chan, H. K.; Mohraz, A. Two-Step Yielding and Directional Strain-Induced Strengthening in Dilute Colloidal Gels. *Phys. Rev. E: Stat., Nonlinear, Soft Matter Phys.* **2012**, *85*, 041403−041406.
(48) Kramb, R. C.; Zukoski, C. F. Yielding in Dense Suspensions: Cage, Bond, and Rotational Confinements. *J. Phys.: Condens. Matter* **2011**, *23*, 035102.
(49) Ahuja, A.; Potanin, A.; Joshi, Y. M. Two Step Yielding in Soft Materials. *Adv. Colloid Interface Sci.* **2020**, *282*, 102179.
(50) Laurati, M.; Egelhaaf, S. U.; Petekidis, G. Nonlinear Rheology of Colloidal Gels with Intermediate Volume Fraction. *J. Rheol.* **2011**, *55*, 673−706.
(51) Liberto, T.; Le Merrer, M.; Manneville, S.; Barentin, C. Interparticle Attraction Controls Flow Heterogeneity in Calcite Gels. *Soft Matter* **2020**, *16*, 9217−9229.
(52) Shih, W. Y.; Shih, W.-H.; Aksay, I. A. Elastic and Yield Behavior of Strongly Flocculated Colloids. *J. Am. Ceram. Soc.* **2004**, *82*, 616−624.
(53) Shih, W.; Shih, W. Y.; Kim, S.; Liu, J.; Aksay, I. A. Scaling Behavior Ofthe Elastic Properties of Colloidal Gels. *Phys. Rev. A* **1990**, *42*, 4772−4779.
(54) Wu, H.; Morbidelli, M. A Model Relating Structure of Colloidal Gels to Their Elastic Properties. *Langmuir* **2001**, *17*, 1030−1036.
(55) Metin, C. O.; Bonnecaze, R. T.; Lake, L. W.; Miranda, C. R.; Nguyen, Q. P. Aggregation Kinetics and Shear Rheology of Aqueous Silica Suspensions. *Appl. Nanosci.* **2014**, *4*, 169−178.
(56) Liberto, T.; Le Merrer, M.; Barentin, C.; Bellotto, M.; Colombani, J. Elasticity and Yielding of a Calcite Paste: Scaling Laws in a Dense Colloidal Suspension. *Soft Matter* **2017**, *13*, 2014−2023.
(57) Whitaker, K. A.; Varga, Z.; Hsiao, L. C.; Solomon, M. J.; Swan, J. W.; Furst, E. M. Colloidal Gel Elasticity Arises from the Packing of Locally Glassy Clusters. *Nat. Commun.* **2019**, *10*, 2237.
(58) Zhou, Z.; Solomon, M. J.; Scales, P. J.; Boger, D. V. The Yield Stress of Concentrated Flocculated Suspensions of Size Distributed Particles. *J. Rheol.* **1999**, *43*, 651−671.
(59) Mewis, J.; Wagner, N. J. *Colloidal Suspension Rheology*; Cambridge University Press, 2012.
(60) Bhagavathi Kandy, S.; Mehdipour, I.; Neithalath, N.; Kumar, A.; Bauchy, M.; Garboczi, E.; Srivastava, S.; Gaedt, T.; Sant, G. Ultrafast Stiffening of Concentrated Thermoresponsive Mineral Suspensions. *Mater. Des.* **2022**, *221*, 110905.
(61) Timmons, J.; Falzone, G.; Balonis, M.; Bauchy, M.; Sant, G. Anomalous Variations in the Viscous Activation Energy of Suspensions Induced by Fractal Structuring. *J. Colloid Interface Sci.* **2018**, *530*, 603−609.
(62) Flatt, R. J.; Houst, Y. F.; Bowen, P.; Hofmann, H.; Widmer, J.; Sulser, U.; Maeder, U.; Bürge, T. A. Adsorption of Superplasticizers on Model Powders: Temperature Dependance, Effect on Zeta Potential and Role of Chemical Structure. *Proceedings of the 10th International Congress on the Chemistry of Cement*; Amarkai AB and Congrex: Göteborg, 1997; Vol. 3.
(63) Sarraf, H.; Havrda, J. Rheological Behavior of Concentrated Alumina Suspension: Effect of Electrosteric Stabilization. *Ceram.-Silik.* **2007**, *51*, 147−152.
(64) Guo, L. C.; Zhang, Y.; Uchida, N.; Uematsu, K. Influence of Temperature on Stability of Aqueous Alumina Slurry Containing Polyelectrolyte Dispersant. *J. Eur. Ceram. Soc.* **1997**, *17*, 345−350.

https://doi.org/10.1021/acs.langmuir.3c00704
Langmuir 2023, 39, 10395−10405